Carbon-based TiO_2 materials for the degradation of Microcystin-LA

Maria J. Sampaio[1], Cláudia G. Silva[1], Adrián M.T. Silva[1,*], Luisa M. Pastrana-Martínez[1], Changseok Han[2], Sergio Morales-Torres, José L. Figueiredo[1], Dionysios D. Dionysiou[2,*], Joaquim L. Faria[1]

[1]*LCM – Laboratory of Catalysis and Materials – Associate Laboratory LSRE-LCM, Faculdade de Engenharia, Universidade do Porto, Rua Dr. Roberto Frias s/n, 4200-465 Porto, Portugal*

[2]*Environmental Engineering and Science Program, University of Cincinnati, Cincinnati, OH 45221, United States*

*Corresponding authors:

adrian@fe.up.pt (A.M.T. Silva); dionysios.d.dionysiou@uc.edu (D.D. Dionysiou).

Abstract

The photocatalytic degradation of a cyanobacterial toxin, microcystin-LA (MC-LA), was studied in aqueous solutions under both simulated solar light and visible light irradiation. Neat TiO_2 and carbon-based TiO_2 materials, prepared with carbon nanotubes (CNT) or graphene oxide (GO), were compared. The highest photocatalytic activity was obtained with a GO-TiO_2 composite comprising 4 *wt.*% of carbon content (GO-TiO_2-4). Complete conversion of MC-LA was achieved under solar light irradiation in 5 min. GO-TiO_2-4 was also active under visible light illumination, with 88% of MC-LA removal in 2 h. The high photocatalytic activity of GO-TiO_2-4 was attributed to the optimal assembly and interfacial coupling between the TiO_2 nanoparticles and the GO sheets that can effectively inhibit electron/hole recombination. Reaction intermediates of MC-LA photocatalytic degradation were also identified by LC/Q-TOF and LC/MS/MS, most of them resulting from the attack of hydroxyl radicals to the MC-LA molecule under solar light irradiation.

Keywords: *photocatalysis; microcystin-LA; graphene oxide; carbon nanotubes; TiO_2.*

1. Introduction

Cyanobacteria (aka, blue-green algae) are a diverse group of photo-autotrophic organisms which can be found in aquatic systems, such as oceans, freshwater lakes, rivers and reservoirs throughout the world [1, 2]. These organisms are essential to the food chain in many ecosystems; however, some species of cyanobacteria can also produce toxic metabolites, which are harmful to human health and ecosystems [3-5]. Microcystins (MCs) are among the most common cyanobacterial toxins found in water and freshwater. The variant microcystin-LR (MC-LR) is the most regularly found and investigated [6]. Other frequently detected variants include MC-YR, MC-RR and MC-LA, which are less studied even though their toxicity has been frequently reported [7, 8]. The structure of MC-LA is similar to MC-LR since these toxins only differ in one amino acid group in their chain, *i.e.*, arginine for MC-LR and alanine for MC-LA [9, 10].The intensification and persistence of MCs in water represents an emerging environmental and health concern. Therefore, the development of efficient water treatment technologies is currently required.

Various studies reported that the application of heterogeneous photocatalysis, using titanium dioxide (TiO_2) as a photocatalyst, may improve the removal of MCs from water [11-13]. In addition, coupling TiO_2 with carbon materials, such as carbon nanotubes (CNT) [14-16] and graphene oxide (GO) [13, 17], have provided a synergistic effect, which can enhance the overall efficiency of the photocatalytic process in particular under visible light illumination.

In previous studies [14, 18, 19], we have found that the efficiency of the photocatalytic process depends on the nature and content of the carbon material used for the preparation of the carbon-based TiO_2 composites. CNT-TiO_2 composites with 20 *wt.*% of the carbon phase revealed to be very efficient for the removal of phenol, methylene blue, caffeine, and diphenhydramine [14, 19, 20]. In the case of GO-TiO_2 composites, the highest efficiency for diphenhydramine degradation was achieved using composites containing 4 *wt.*% of GO [21]. However, only a

few studies have been focused on the degradation of MCs with carbon-based photocatalysts. For instance, in a recent work, Fotiou et al. [22] studied the degradation of MC-LR under both UV-A and solar light irradiation in the presence of graphene-based composites (GO-TiO_2) and proved that the combination of GO with TiO_2 leads to an increase in the efficiency of MC-LR removal when compared with the bare material (TiO_2).

Taking into consideration these previous findings, a composite containing 4 *wt.*% of GO (GO-TiO_2-4) and others comprising 4 *wt.*% and 20 *wt.*% of oxidized CNT (CNT-TiO_2-4 and CNT-TiO_2-20, respectively) are compared in the photocatalytic degradation of MC-LA under visible and simulated solar light irradiation for the first time in this study. Insights on the identification of the resulting intermediate products are also given.

2. Experimental

2.1. Carbon materials preparation

Natural graphite (purity > 99.9995%, Sigma–Aldrich) was oxidized using the modified Hummers´ method, as described elsewhere [21, 23]. Then the oxidized material was dispersed in water and exfoliated under sonication for 1 h. Finally, the non-exfoliated graphite oxide was removed by centrifugation and a GO aqueous dispersion was obtained.

Multi-walled carbon nanotubes (CNTs > 95% purity, purchase from Shenzhen Nanotechnologies Co. Ltd) were oxidized with a 10 M HNO_3 solution (purity > 65 %, Fluka) at boiling temperature for 3 h. The suspension was washed several times, until neutrality of the rinsing waters. The CNTs were recovered and dried for 12 h at 383 K.

2.2. Preparation of carbon–based TiO_2 composites

The different amounts of oxidized CNTs were dispersed in distilled water and sonicated for 30 min. The carbon-TiO_2 composites were prepared by liquid phase deposition method, as described elsewhere [21]. Briefly, 0.1 M of TiO_2 precursor ($(NH_4)_2TiF_6$ purity > 99.99 %,

Sigma-Aldrich) and 0.3 M of H_3BO_3 (purity > 99.5 %, Fluka) were added to the carbon material suspensions and heated at 333 K for 2 h under continuous stirring. The resulting materials were washed and dried at 373 K for 2 h under vacuum followed by a calcination step under N_2 flow at 473 K. The composites were labeled as CNT–TiO_2-X and GO–TiO_2-X, where X corresponds to the carbon load used (4 *wt*.% or 20 *wt*.%). Bare TiO_2 was also prepared following the same procedure but without the addition of carbon material.

2.3. Characterization of TiO_2 nanostructured composites

The thermogravimetric (TG) analysis of the prepared materials was performed by heating the sample from 323 K to 1273 K at 20 K min^{-1} under air flow using a STA 490 PC/4/H Luxx Netzsch thermal instrument. The N_2 adsorption-desorption isotherms at 77 K were measured on a Quantachrome NOVA 4200e apparatus. The BET specific area (S_{BET}) was obtained from the N_2 adsorption data in the relative pressure range 0.05-0.20. The total volume of N_2 adsorbed (V_p) was also calculated according to the Gurvitch's rule [24, 25].

Temperature programmed desorption (TPD) analysis was performed using an AMI-300 Catalyst Characterization Instrument (Altamira Instruments). The samples were heated to 1073 K at 5 K min^{-1} under helium flow.

The morphology of the materials was analyzed by scanning electron microscopy (SEM) using a Philips XL 30 ESEM-FEG apparatus. Transmission electron microscopy (TEM) was performed in a Philips CM20 equipment.

The diffuse-reflectance UV–Vis spectra (DRUV-Vis) of the materials were measured on a JASCO V-560 UV-Vis spectrophotometer equipped with an integrating sphere attachment (JASCO ISV-469).

A Fourier Transformed Infrared spectrophotometer (FT-IR, Nicolet 510-P) equipped with a Pike ATR (attenuated total reflection) accessory with a high-pressure clamp and a ZnSe crystal plate was used for the surface characterization of the materials.

2.4. Photocatalytic setup

The photocatalytic degradation MC-LA was evaluated under visible and simulated solar light irradiation. The experiments were carried out under natural conditions (pH = 5.7) in a borosilicate glass petri dish (Pyrex, diameter = 60 mm, length = 15 mm) sealed with a cover and air-cooled using appropriate fans to avoid solution evaporation. An initial concentration of 0.2 μM MC-LA (99.3%, CalBiochem) was prepared using Milli-Q water and the concentration of photocatalyst was 0.5 g L^{-1}. Total volume of the solution was 10 mL in the reactor. This concentration was selected by taking into consideration the guidance values for the relative probability of acute effects to human health and ecosystems during the exposure to cyanobacteria (~ 0.02 to 2.2 μM) according to the World Health Organization (WHO) [26].

A Xenon lamp (OF 300W 67005, Newport, Oriel Instrument) was used to simulate solar light irradiation (light irradiance of 47.1 mW cm^{-2}). For the experiments under visible light, two 15 W fluorescent lamps (Cole-Parmer) with a UV block filter (UV420, Opticology) were applied as irradiation source (irradiance of 0.4 mW cm^{-2}). The photocatalytic experiments were carried out in triplicate for each catalyst. Experiments in the absence of catalyst were also performed to determine the contribution from direct photolysis. It was found that the photocatalytic oxidation of the MC-LA can be described by a pseudo-first order kinetic model, according to the following equation:

$$C = C_0 e^{-k_{app} t} \quad (1)$$

where C corresponds to MC-LA concentration, k_{app} is the pseudo-first order kinetic constant, t is the reaction time and C_0 is the initial MC-LA concentration at $t = 0$. The values of k_{app} were obtained by non-linear regression.

2.5. Analytical techniques

Samples were analyzed using a high-performance liquid chromatograph (HPLC, Series 1100, Agilent) with a photodiode-array detector (PDA) set at 238 nm and using a C_{18} Discovery HS (Supelco) column (150 mm × 2.1 mm, 5 μm particle size). The method starts with a mobile phase consisting of 0.05% (v/v) trifluoroacetic (TFA) acid in Milli-Q water (A) and 0.05% TFA in acetonitrile (B) in a ratio of (75:25) followed by a linear gradient step to A:B (30:70) in 6 min; finally the initial conditions were re-established in 1 min gradient step and the A:B (75:25) mixture was isocratically eluted for 5 min. The analysis was performed with a column temperature of 313 K, a flow rate of 0.2 mL min^{-1} and an injection volume of 50 μL.

Identification of intermediates was performed using a combination of liquid chromatography with a quadrupole time-of-flight (LC/Q-TOF) as well as with mass spectrometry (LC/MS/MS) in an Agilent G6540A apparatus. LC/Q-TOF was used to obtain molecular weight and formula information, and LC/MS/MS was used to determine further structural information. MS/MS data were acquired using the same instrument in targeted MS/MS mode. For both Q-TOF and MS/MS modes, the same LC method was used, namely an Agilent Eclipse XDB-C18 column (2.1 mm × 50 mm, 3.5 micron), with an isocratic elution mode A:B (95:5) in 5 min (where solvent A is 0.1% formic acid in water and solvent B is 0.1% formic acid in acetonitrile) and a flow rate set at 0.2 mL min^{-1}.

3. Results and Discussion

3.1 Thermogravimetric analysis and surface area

The carbon content (*wt.*%) in the composite materials was determined by thermogravimetric analysis; both neat TiO_2 and the composites were submitted to a thermal treatment under air and the weight loss was monitored. The carbon content in the composite corresponds to the difference between the weight loss observed for the composite and that of neat TiO_2. The obtained results are in a good agreement with the nominal carbon content (i.e. 4 *wt.*% or 20

wt.% depending on the composite) which indicate that no appreciable degradation of the carbon phase occurred during the calcination step.

The BET specific area (S_{BET}) and the respective total pore volume (V_p) of TiO_2, CNT, GO as well as of the carbon-based TiO_2 composites were obtained from the N_2 adsorption isotherms are shown in Table 1. Different tendencies were observed for the composites depending on the type of carbon material used. The results show that V_p and S_{BET} are comparable for GO-TiO_2-4 (0.17 cm^3 g^{-1} and 110 m^2 g^{-1}, respectively) and neat TiO_2 (0.11 cm^3 g^{-1} and 118 m^2 g^{-1}, respectively), and higher than for GO (0.003 cm^3 g^{-1} and 21 m^2 g^{-1}, respectively); this is related to agglomeration of GO sheets during the necessary drying process in order to perform N_2 adsorption analysis.

Generally, anchoring and dispersion of the TiO_2 particles on CNT is promoted when functional groups are introduced on CNT by oxidation treatments, avoiding agglomeration of TiO_2 and thus increasing the surface area [12, 15]. However, results show that the presence of a small amount of CNT (4 *wt.*%) in the composite leads to a marked decrease in S_{BET} with relation to both TiO_2 and CNT phases. A similar behavior was observed in a previous work where the effect of CNT load on CNT-TiO_2 composites was assessed [14]. The decrease of S_{BET} was attributed to the competitive anchoring and agglomeration of TiO_2 crystallites on the sidewalls of CNTs, leading to the formation of bigger TiO_2 particles than in neat TiO_2. The introduction of a larger amount of CNTs resulted in an increase of the surface area (S_{BET} = 152 m^2 g^{-1} and V_p = 0.48 cm^3 g^{-1} for CNT-TiO_2-20). A higher CNT content, i.e. a higher amount of hydrophilic surface chemical groups, enhances the dispersion of the TiO_2 particles thus increasing the surface area.

Table 1. BET specific area and total pore volume of the materials.

Sample	S_{BET} (m^2 g^{-1})	V_p (cm^3 g^{-1})
GO	21	0.003
CNT	155	0.61
TiO_2	118	0.11
GO-TiO_2-4	110	0.17
CNT-TiO_2-4	59	0.15
CNT- TiO_2-20	152	0.48

3.2. SEM and TEM analysis

SEM analysis was performed for the visualization of the morphology of the different materials. Representative SEM micrographs of neat TiO_2 (Fig. 1a), GO-TiO_2-4 (Fig. 1c), CNT-TiO_2-4 (Fig. 1e) and CNT-TiO_2-20 (Fig. 1g) clearly reveal the differences in the morphology of the materials. In the case of neat TiO_2 (Fig. 1a), spherical-like TiO_2 particles aggregate to form larger particles (as confirmed at higher magnifications, Fig. 1a inset). Images of GO-TiO_2-4 (Fig. 1c) show a good dispersion of TiO_2 particles on both sides of the GO layers. In the case of CNT-TiO_2 materials (Fig. 1e and Fig. 1g), clusters of TiO_2 particles surrounding CNT are observed.

TEM micrographs of the materials are also shown in Fig. 1. These images corroborate the previous observations by SEM. TEM image of the GO-TiO_2-4 composite (Fig. 1d) indicates that TiO_2 particles grow around the GO layers, showing a good self-assembly of the TiO_2 nanoparticles on GO. For CNT-TiO_2 composites, some differences are observed between the materials prepared with different carbon load. CNT are hardly seen by TEM analysis in the case of CNT-TiO_2-4 (Fig. 1f), maybe because some CNT are embedded into big TiO_2 agglomerates, while TiO_2 particles are dispersed along the sidewalls of CNT in the case of CNT-TiO_2-20 (Fig. 1h). These observations are in line with their S_{BET}, the strong agglomeration of the TiO_2 particles in CNT-TiO_2-4 resulting in a lower surface area.

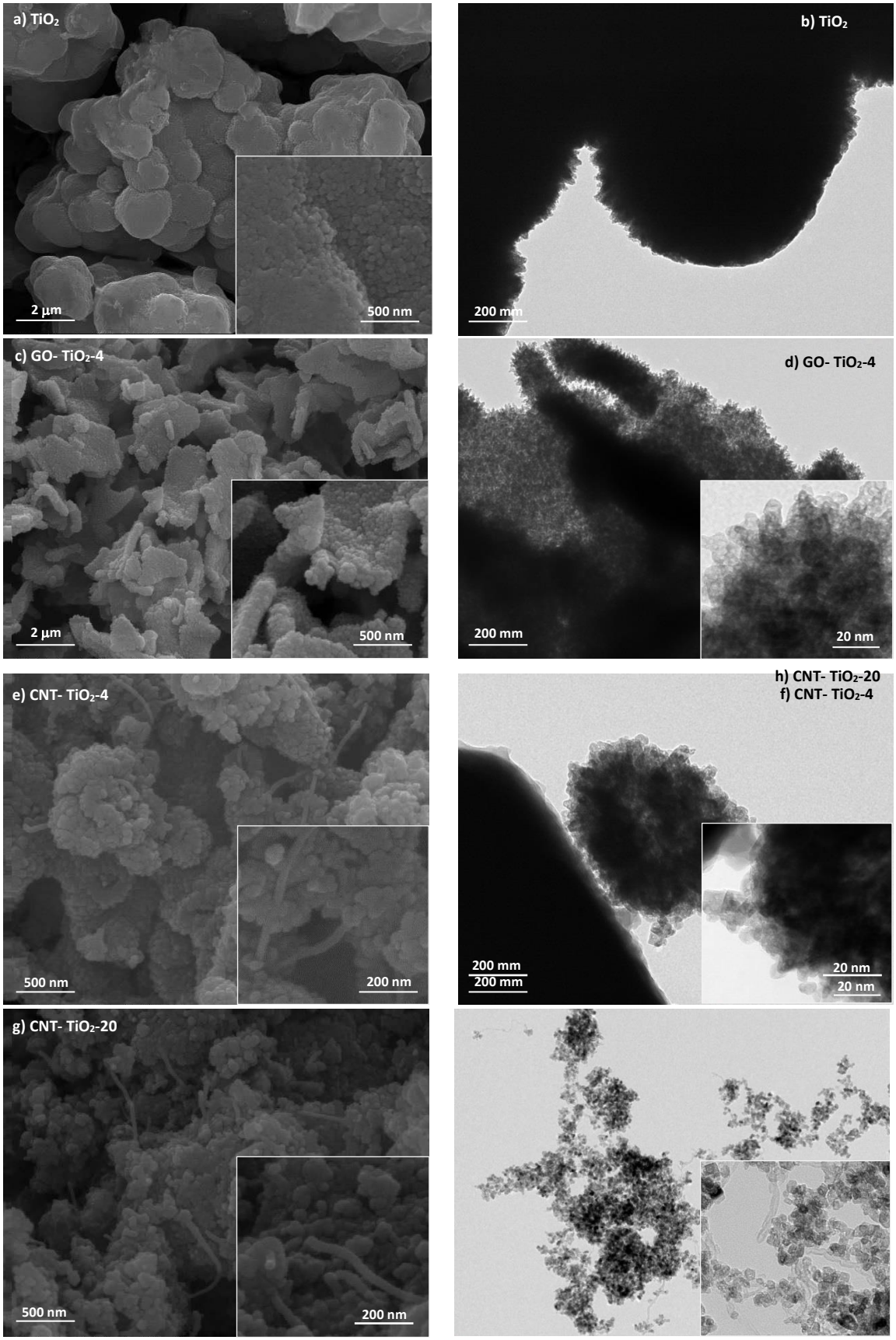

Fig. 1. SEM (a, c, e, g) and TEM (b, d, f, h) images of neat TiO_2 (a, b), GO-TiO_2-4 (c, d), CNT-TiO_2-4 (e, f) and CNT-TiO_2-20 (g, h).

3.3 DRUV-Vis spectroscopy analysis

The diffuse reflectance UV-Vis spectra of TiO_2 and of the carbon-based TiO_2 materials are depicted in Fig. 2.

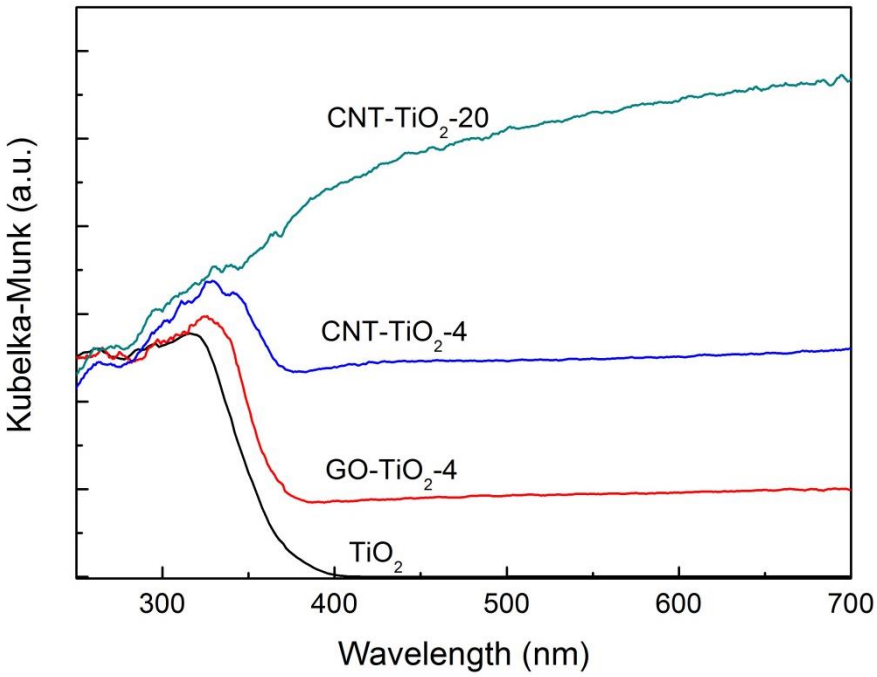

Fig. 2. DRUV-Vis spectra of neat TiO_2 and carbon-based TiO_2 materials.

Neat TiO_2 shows the characteristic absorption sharp edge rising at 400 nm due to the bandgap transition of the semiconductor, while the carbon-based TiO_2 composites show absorption in the full spectral range. The increase in absorption shown by carbon-TiO_2 composites, mostly in the visible spectral range, has been ascribed in previous studies to the inherent light absorption capacity of carbon materials and also to the possibility of being photoexcited, in this way promoting electronic transitions between carbon and TiO_2 phases [14, 21]. This increase in light absorption is normally proportional to the carbon content, as observed for CNT-TiO_2-4 and CNT-TiO_2-20. For the composites prepared with different carbon sources but with the same carbon content, CNT-TiO_2-4 and GO-TiO_2-4, the higher absorption observed in the visible range for the former can be attributed to some phase segregation, as observed in Fig. 1e, with the prevalence of visible light absorption by naked CNT. In the case of GO-TiO_2-4, microscopy

results (Figs. 1c and 1d) show that GO sheets are uniformly covered by TiO_2. This good assembly between carbon and TiO_2 phases is normally an important requirement for enhanced charge mobility in this type of composite materials upon photoexcitation [14].

3.4. ATR infrared analysis

ATR-FTIR spectra of neat TiO_2, CNT, GO and the respective carbon-based TiO_2 composites are depicted in Fig. 3. The ATR spectrum recorded for neat TiO_2 shows mainly a broad band situated between 2500 and 3600 cm^{-1}, associated with stretching vibrations of hydrogen bonded surface water molecules and hydroxyl groups. This is confirmed by the presence of some weak bands around 1630 cm^{-1} caused by bending vibration of coordinated water as well as from the Ti-OH group [27, 28]. The spectra of neat TiO_2 and all the carbon-based TiO_2 composites show a characteristic band associated to TiO_2 materials (between 800 and 950 cm^{-1}), corresponding to Ti-O-Ti bonds [29].

In the case of GO, a broad band situated around 3000-3500 cm^{-1} is assigned to the vibration of C-OH groups. The absorption band at 1720 cm^{-1} is attributed to carbonyl groups, C=O. The band at around 1300-1370 cm^{-1} corresponds to C-OH stretching. The band at 1220 cm^{-1} corresponds to breathing vibrations of epoxy groups (-O-) and the band at 1050 cm^{-1} is attributed to the stretching vibration of C-O groups [17]. The intensity of the peak associated to C-O (hydroxyl and epoxy) decreased significantly in the GO-TiO_2-4 composite, suggesting TiO_2 anchoring to GO preferentially through these sites. The absorption band at around 1600 cm^{-1} can be assigned to the skeletal vibration of graphene sheets.

A peak was observed at 1530-1560 cm^{-1} in the CNT spectrum (Fig. 3 inset), indicating the existence of carbon double bonds (C=C) and confirming the hexagonal-ring structure of the CNT walls. The presence of the peak at 1720 cm^{-1} corresponds to the stretching vibration of carbonyl groups (C=O), generated by the oxidation treatment performed over pristine CNT.

The lower peak intensities in the CNT spectrum in comparison with the GO spectrum suggest the presence of larger amounts of oxygen surface groups in GO.

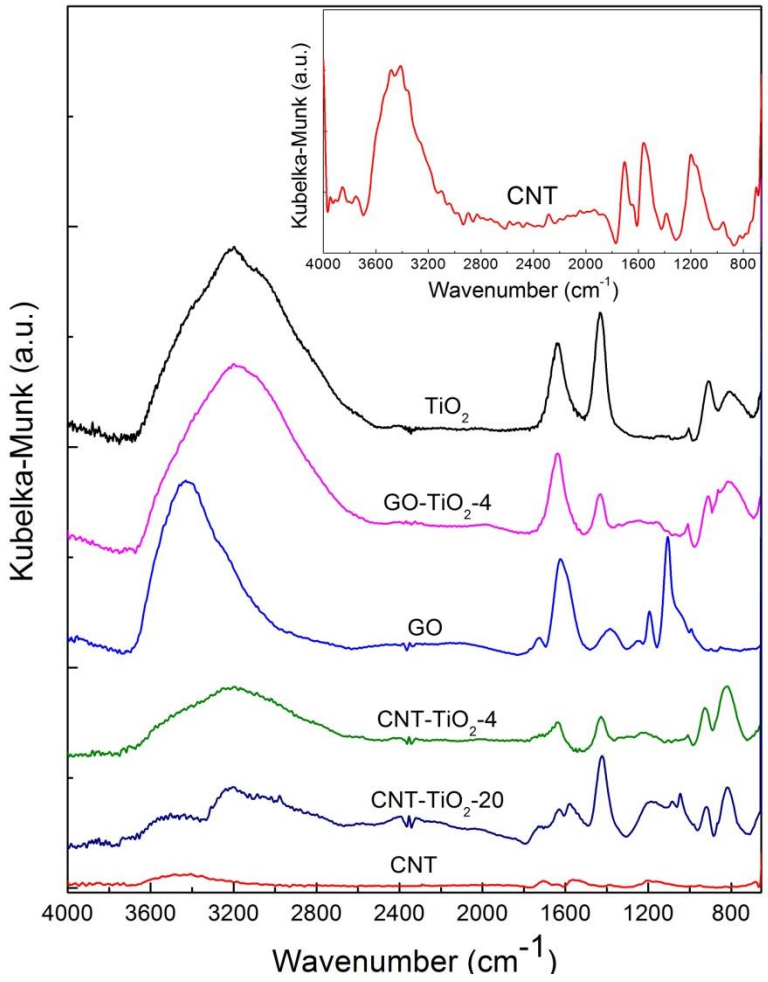

Fig. 3. ATR spectra of neat TiO_2, CNT, GO and respective carbon-based TiO_2 composites.

3.5 Temperature programmed desorption (TPD)

The surface chemistry of GO and CNT was modified by introducing oxygenated surface groups during the oxidation treatments. In general, the presence of oxygenated groups improves the interaction between the carbon phase and TiO_2 particles by the formation of Ti–O–C bonds and promoting TiO_2 dispersion during the synthesis procedure.

TPD analysis was used for the determination and quantification of chemical oxygen species present at the surface of the GO and oxidized CNT. Oxygen surface groups on carbon materials

are thermally decomposed into CO and CO_2, being possible to identify and quantify particular functional groups from TPD spectra [30, 31].

Fig. 4a and Fig. 4b show the TPD profiles of the groups evolved respectively as CO and CO_2 from the surface of the carbon materials used in this work. The oxygen amounts evolved during the TPD experiments are significantly larger for GO (23.6 *wt.*%) than for CNT (ca. 3.1 *wt.*%). These larger amounts of CO and CO_2 detected for GO (4156 and 5305 μmol g^{-1}, respectively), in comparison to CNT (1066 and 434 μmol g^{-1}, respectively), correspond to a larger amount of oxygen surface groups. This can be related with the less severe oxidation treatment performed over CNT in comparison to that used over GO.

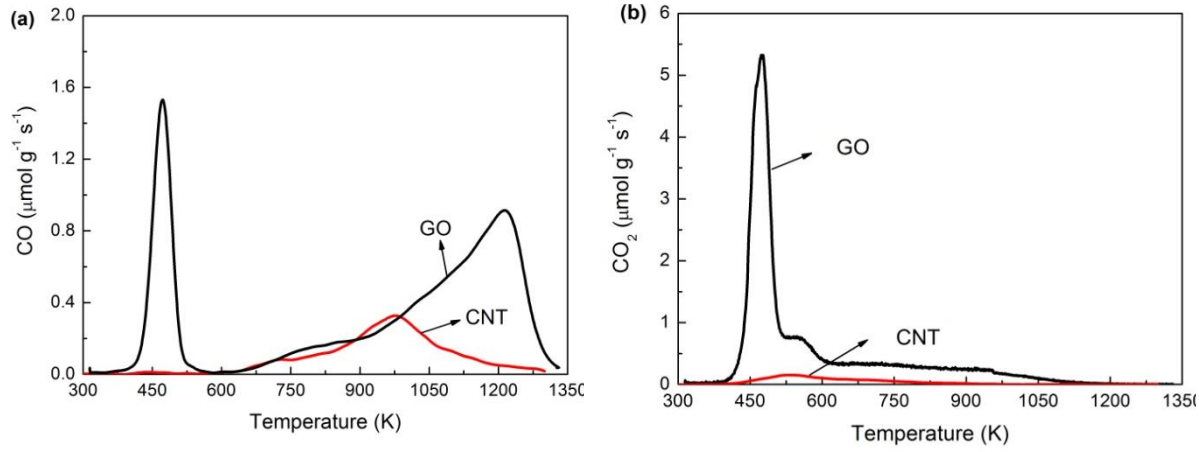

Fig. 4. TPD profiles of GO and CNT: (a) CO and (b) CO_2 release.

Regarding the CO and CO_2 spectra obtained for the GO sample, it is noteworthy the presence of an intense peak at low temperature (~471 K) assigned to the epoxy and hydroxyl groups located on basal planes of GO, as previously reported [32, 33]. The CO profile (Fig. 4a) shows other oxygen surface groups, including carboxylic acids/~510-570K, carboxylic anhydrides/~710-790 K, phenols/~900-950 K, and carbonyl/quinone groups/~1060-1300 K. Regarding the CO_2-TPD spectra (Fig. 4b), carboxylic acids groups/~500-550 K, as well as anhydride groups/~600-760 K and lactone groups/~880-980 K were also incorporated [15, 32].

The high oxygen content on the GO surface can explain its high dispersion in the solution during the preparation of the GO-TiO_2-4 composite, as well as the good assembly of the TiO_2 particles on GO (Fig. 1b). The TPD analysis is also in agreement with the results of ATR spectroscopy (Fig. 3), in which more intense peaks were observed for the GO-TiO_2 material, in comparison with CNT-TiO_2 composites, due to the higher amount of oxygen groups in GO.

3.6. Photocatalytic degradation of MC-LA

Neat TiO_2 and carbon-based TiO_2 composites were tested in the photocatalytic degradation of MC-LA. In order to understand the photo-induced degradation reaction and the role played by the carbon materials in the photocatalytic process, composites were used under simulated solar light and visible light irradiation. Blank experiments under both irradiation conditions and in the absence of any catalyst were also performed for comparison purposes. MC-LA is a very light-stable contaminant, since direct photolysis, i.e., in the absence of a photocatalyst, is negligible under both simulated solar light (Fig. 5a) and visible light irradiation (Fig. 5b).

Control experiments under dark conditions (absence of light) were also performed to evaluate the extent of adsorption of MC-LA on the tested materials (Fig. 5c and 5d). All the photocatalytic and adsorption experiments were performed independently. Results show that the adsorption equilibrium is established after 60 min for all the photocatalysts tested, as previously confirmed by performing dark adsorption runs for 5 h (not shown).

Figs. 5a and 5c show a synergistic effect between the carbon phase and TiO_2 particles, but the magnitude of this effect depends on the nature and content of the carbon material. Among the photocatalysts containing 4 *wt*.% of carbon phase, the highest photocatalytic performance under simulated solar light was found for the GO–TiO_2-4 composite (k_{app} = 116×10^{-2} min^{-1}). The results revealed that after 5 min of solar light irradiation, the GO-TiO_2-4 composite produced the complete removal of MC-LA, while this was achieved only after 90 min with neat TiO_2. The synergistic effect could be attributed to the interfacial charge transfer process that can

effectively inhibit electron−hole recombination, allowing GO-TiO_2-4 to generate a higher amount of reactive radicals when compared with neat TiO_2 [18, 22]. Also, the good assembly and interfacial coupling between GO and TiO_2 particles, as observed by SEM and TEM (Fig, 1c and 1d, respectively), could explain the high efficiency of the GO-TiO_2-4 composite.

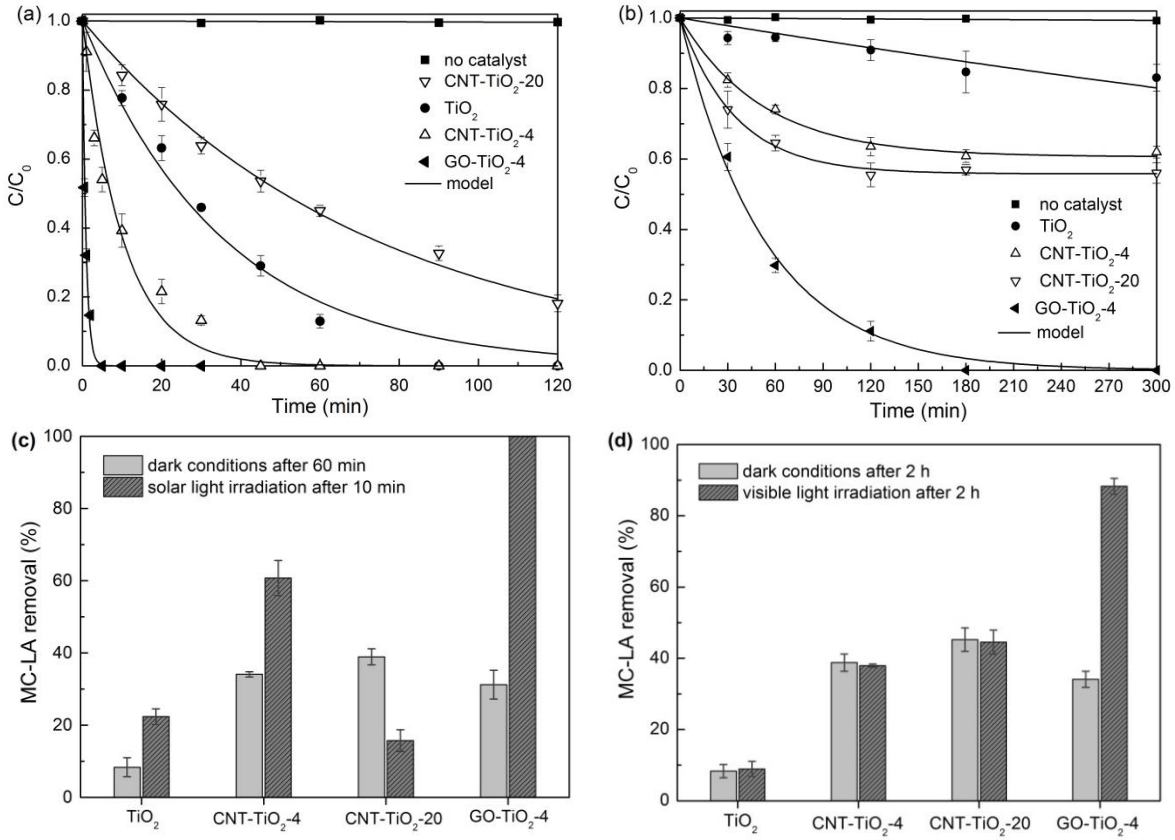

Fig. 5. Normalized concentration of MC-LA (C/C_0) using neat TiO_2 and carbon-based TiO_2 composites under simulated solar light (a) and under visible light (b) irradiation. Respective photolysis (no catalyst) is also shown for comparison. MC–LA removal (%) in dark conditions and under simulated solar light (c) and under visible irradiation (d).

Regarding the CNT-TiO_2 composites, in our previous studies it was found that 20 *wt*.% of CNT was the optimal load for the degradation of different organic compounds [14, 15], yet using different preparation methods for the synthesis of the CNT-TiO_2 composites. In fact, CNT-TiO_2

composites with different carbon loads have been investigated in a number of studies [14, 16]. In most cases TiO_2 nanoparticles were loaded onto or randomly mixed with CNTs, and the photocatalytic activity of the resulting materials increased with the CNT content up to optimal value and then decrease.

In the present work, results show an increase in k_{app} (9.87×10^{-2} min^{-1}) for the CNT-TiO_2 composites containing 4 *wt*.% of CNT, when compared with neat TiO_2 (2.77×10^{-2} min^{-1}) under simulated solar light. However, the increase of the CNT load to 20 *wt*.% (CNT-TiO_2-20) led to a decrease in the efficiency of MC-LA removal compared with neat TiO_2. This different behavior can be attributed to the different physical-chemical, morphological and optical properties of the composites resulting from different synthesis procedures, which will influence the photoefficiency of the resulting materials. The weak interaction between the CNT and TiO_2 particles would clearly affect the interfacial charge transfer process that can effectively inhibit electron-hole recombination. These results underline the importance of controlling the carbon load and the preparation method of the composites in order to achieve an optimal synergistic interaction between the carbon material and TiO_2.

The photocatalytic activity of the carbon-based TiO_2 composites for the degradation of MC-LA under visible light irradiation was also evaluated (Fig. 5b). Once again, the results show that the GO-TiO_2-4 composite exhibited the highest photocatalytic activity, with 88% removal of MC-LA after 120 min and complete conversion after 180 min (k_{app} = 1.87×10^{-2} min^{-1}). These results can be attributed to the role of GO as photosensitizer, enabling electron transfer to TiO_2 upon visible excitation. The activity of neat TiO_2 was negligible at such conditions due to its low absorption in the visible spectral range (λ > 400 nm). For CNT-TiO_2-4 and CNT-TiO_2-20 composites, results reveal that the removal of MC-LA under visible light was mostly due to the adsorption of MC-LA on these materials. CNTs normally enhance the activity of TiO_2 due to their structural and electronic properties [14, 34]. However, a different behavior was found in the degradation of MC-LA under visible light. The negligible photocatalytic activity observed

can be attributed to the very low amount of oxygen surface groups that leads to a weak interaction between TiO_2 and CNT.

3.2. MC-LA reaction intermediates using neat TiO_2 and GO-TiO_2 photocatalysts

The above results proved that GO-TiO_2-4 is an excellent photocatalyst for the degradation of MC-LA. Complete degradation of this pollutant was achieved under both simulated solar light and visible light irradiation. The identification of intermediate products has been performed for obtaining information about the MC-LA photocatalytic degradation mechanism. An appreciable number of reports have examined the degradation pathway of MC-LR [35-37], but no reports are found for the degradation of MC-LA. Nevertheless, the structural similarity between both molecules, since they only differ in one amino acid group (arginine for MC-LR and alanine for MC-LA), can be useful for the determination of primary MC-LA intermediates. These intermediates were identified by LC-MS/MS in experiments performed with neat TiO_2 under simulated solar light and with GO-TiO_2-4 under both simulated solar light and visible light irradiation. Before identifying the primary intermediates, a scan of the total ion chromatogram (TIC) was performed and distinct peaks were observed. Table 2 summarizes the products that were detected during the photocatalytic degradation of MC-LA in terms of their molecular formula, mass-to-charge ratio (*m/z*) and retention times (R_t), using the different catalysts.

Table 2. Reaction intermediates observed for MC-LA degradation using neat TiO_2 and GO-TiO_2-4 photocatalyst under simulated solar [(a)] and visible light [(b)] irradiation.

Formula	Peak (*m/z*)	R_t (min)	Catalyst
$C_{46}H_{67}N_7O_{12}$	910.5 (MC-LA)	3.74	-

$C_{35}H_{69}N_5O_{14}$	784.5	2.62	$^{(a)}TiO_2$, $^{(a)}GO\text{-}TiO_2$-4
$C_{46}H_{69}N_7O_{15}$	960.5	2.90 3.01	$^{(a)}TiO_2$
$C_{43}H_{67}N_7O_{11}$	858.5	3.16	$^{(a)}TiO_2$, $^{(a)}GO\text{-}TiO_2$-4
$C_{45}H_{67}N_7O_{12}$	898.5	3.16 3.27	$^{(b)}GO\text{-}TiO_2$-4
$C_{45}H_{67}N_7O_{13}$	914.5	3.16 3.25 3.43	$^{(b)}GO\text{-}TiO_2$-4
$C_{42}H_{65}N_7O_{13}$	812.5	3.40	$^{(b)}GO\text{-}TiO_2$-4
$C_{45}H_{69}N_7O_9$	916.5	3.14 3.75	$^{(a,b)}GO\text{-}TiO_2$-4
$C_{46}H_{69}N_7O_{13}$	926.5	3.23 3.35 3.53	$^{(a)}TiO_2$, $^{(a,b)}GO\text{-}TiO_2$-4
$C_{46}H_{69}N_7O_{14}$	944.5	3.21 3.56	$^{(a)}TiO_2$, $^{(a,b)}GO\text{-}TiO_2$-4
$C_{43}H_{65}N_7O_{10}$	840.5	3.42	$^{(a)}TiO_2$, $^{(a,b)}GO\text{-}TiO_2$-4
$C_{45}H_{65}N_7O_{10}$	864.5	3.75	$^{(a,b)}GO\text{-}TiO_2$-4
$C_{44}H_{71}N_3O_{15}$	882.5	3.78	$^{(b)}GO\text{-}TiO_2$-4
$C_{44}H_{65}N_4O_9$	836.5	3.82	$^{(b)}GO\text{-}TiO_2$-4
$C_{45}H_{69}N_3O_{14}$	876.5	3.83	$^{b}GO\text{-}TiO_2$-4

The most intense peaks, corresponding to *m/z* = 926.5 and *m/z* = 944.5, were observed for reactions using either TiO_2 or GO-TiO_2-4 composites with both irradiation systems. Multiple peaks in the TIC were observed for these intermediates, which can represent stereoisomers (differing in the three-dimensional orientation of the bonds) or structural isomers with

completely different structures. Two peaks were also observed for the *m/z* = 898.5, 916.5 and 960.5.

Under simulated solar light, the majority of the intermediates detected were produced within the first 2 min of irradiation when using the GO-TiO_2-4 composite. A negligible number of intermediates were detected after 10 min, which seems to be attributed to their subsequent and rapid oxidation during the photocatalytic reaction. Nearly the same intermediates were identified when the neat TiO_2 photocatalyst was used under simulated solar light; however, the oxidation of these intermediates was slower in this case.

Under visible light illumination, complete conversion of MC-LA was obtained in 180 min when using the GO-TiO_2-4 composite, but the reaction was much slower than that observed with simulated solar light and, as consequence, more intermediates were detected with visible light illumination.

As mentioned before, MC-LA has a similar structure to MC-LR, consisting of seven amino acid chains, with the Adda (3-amino-9-methoxy-2,6,8-trimethyl-10-phenyl-4,6-decadienoic acid) side chain being largely responsible for the MCs toxicity [38]. Taking into account this information and that already reported in literature [36, 39], a preliminary structural elucidation of the MC-LA degradation pathway is proposed (Fig. 6).

Antoniou *et al.* [36] studied the MC-LR (*m/z* = 995.5) degradation pathway under UV irradiation and observed a peak corresponding to *m/z* = 1011.5, which has been attributed to the addition of a hydroxyl radical ($HO^{\bullet}$) to one of the aromatic double bonds. Several studies dealing with biomolecules showed that the hydroxylation of aromatic rings is a very common phenomenon [36, 40]. In the case of the photocatalytic degradation of MC-LA (*m/z* = 910.5), using both TiO_2 and GO-TiO_2-4 photocatalysts, an intermediate with a difference of 16 in the *m/z* value was detected, which seems to indicate that the aromatic ring undergoes hydroxyl substitution ($HO^{\bullet}$) of a hydrogen to form the *m/z* = 926.5 (Fig. 6A). The presence of isomers of

the intermediate *m/z* = 926.5 seems to indicate that the hydroxylation can occur at different positions of the aromatic ring.

Another main intermediate detected corresponds to *m/z* = 944.5 (an *m/z* difference of 34 between MC-LA and the intermediate), which can indicate a HO• radical attack at either double bond C_4-C_5 or C_6-C_7 on the Adda chain (Fig. 6B). In studies with MC-LR, this site has been considered as the most prone to be attacked by HO• radicals due to its position [22, 36, 41]. Antoniou *et al.* reported [36] that *m/z* = 1029.5 formation starts with the HO• radical reacting with the diene bonds to produce adducts through the hydroxyl addition and hydroxyl substitution. In our case, the intermediate with *m/z* = 944.5 detected in the degradation of MC-LA seems to correspond to the analogue *m/z* = 1029.5 observed in the degradation of the MC-LR.

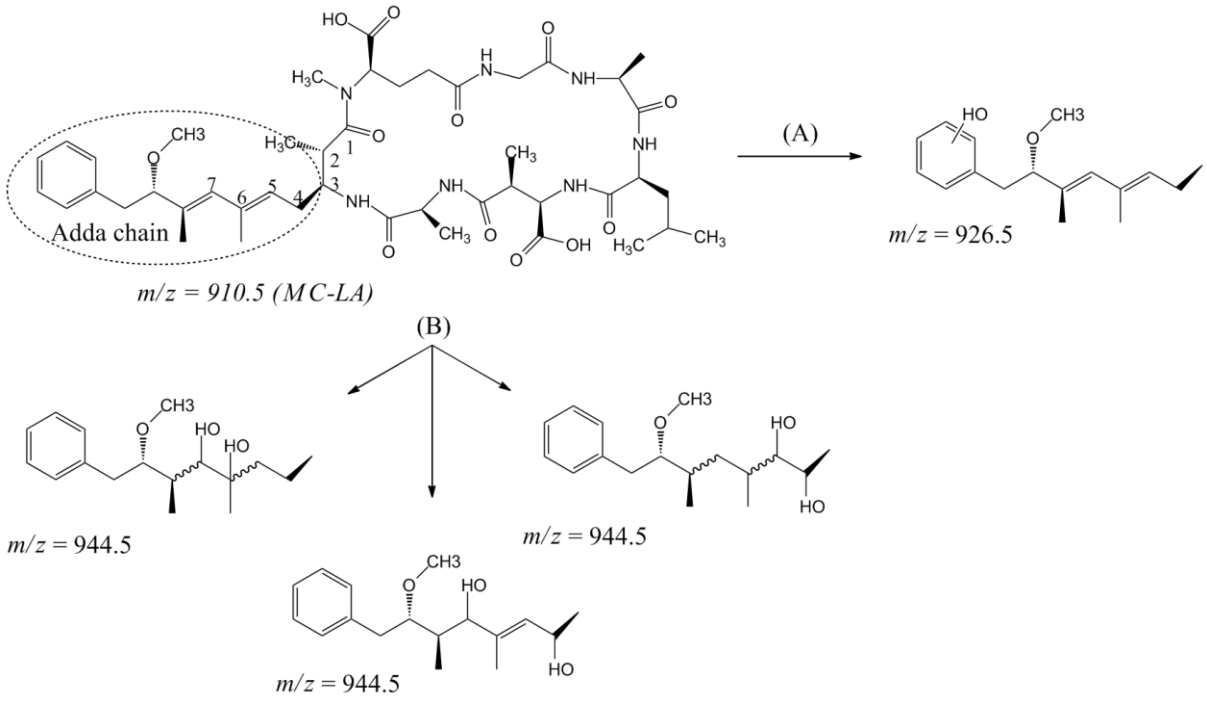

Fig. 6. (A) Attack of hydroxyl radicals on the aromatic ring of MC-LA. (B) Attack of hydroxyl radicals on the conjugated carbon double bonds of MC-LA Adda chain.

Although, the reaction mechanism seems to be mostly driven by HO• radical attack, the formation of reactive species such as radical superoxide anion ($O_2^{\bullet-}$) and singlet oxygen ($^1O_2$)

may assume a more important role in the photocatalytic mechanism under visible light irradiation [42], which may rationalize the presence of intermediates that were not detected under simulated solar light irradiation. In the present work, the reaction mechanism proposed for the preliminary steps of MC-LA photocatalytic transformation under simulated solar light irradiation seems to follow a similar route to that proposed by Antoniou *et al.* [36] for the photocatalytic degradation of MC-LR when using TiO_2.

Further studies are now required, using advanced analytical techniques, for exact identification of all reaction intermediates of MC-LA photocatalytic degradation under different operating conditions.

Conclusions

The photocatalytic degradation of the cyanotoxin MC-LA under simulated solar light and visible light irradiation was achieved by using carbon-based TiO_2 composites containing 4 wt.% and 20 wt.% of GO and CNT as carbon phase. Neat TiO_2 was used as reference.

The efficiency of the photocatalytic process depends on the nature and content of the carbon material used. Among the photocatalysts used, GO-TiO_2-4 exhibited the highest photocatalytic activity under simulated solar light and visible light irradiation. The excellent performance of the GO-TiO_2-4 composite can be attributed to the optimal self-assembly between GO and TiO_2 particles. The MC-LA removal observed with CNT-containing composites under visible light irradiation was mostly due to adsorption on the composite material rather than due to photocatalytic degradation. Preliminary insights to identify MC-LA intermediates are shown for neat TiO_2 and GO-TiO_2-4, under both irradiation conditions. Results suggest that photocatalytic degradation mechanism takes place mostly via hydroxyl radical attack under simulated solar light irradiation.

Overall, this study shows that the GO-TiO_2-4 composite is an efficient photocatalyst for the degradation of MC-LA in water under simulated solar light and also under visible light

irradiation, being a promising material for the detoxification of cyanotoxin-contaminated surface water and freshwaters.

Acknowledgements

Financial support for this work was provided by project PTDC/AAC-AMB/122312/2010 co-financed by FCT (Fundação para a Ciência e a Tecnologia) and FEDER (ERDF - European Regional Development Fund) through Programme COMPETE (FCOMP-01-0124-FEDER-019503), and partially by PEst-C/EQB/LA0020/2013 (financed by FCT and FEDER through COMPETE) and NORTE-07-0162-FEDER-000050, NORTE-07-0124-FEDER-000015 and NORTE-07-0202-FEDER-038900 (financed by QREN, ON2 and FEDER). FCT is also acknowledged for the grants SFRH/BD/79878/2011 (MJS), SFRH/BPD/74239/2010 (SMT) and SFRH/BPD/88964/2012 (LMPM) and the IF/01501/2013 contract (AMTS) under the FCT Investigator 2013 Programme with financing from the European Social Fund and the Human Potential Operational Programme. CH acknowledges the Graduate School Dean's Fellowship. The US National Science Foundation (US-Ireland collaborative research CBET (1033317)) and the Cyprus Research Promotion Foundation through Desmi 2009-2010 which is co-financed by the Republic of Cyprus and the European Regional Development Fund of the EU under contract number NEA IPODOMI/STRATH/0308/09 are also acknowledged.

References

[1] H.W. Paerl, N.S. Hall, E.S. Calandrino, Controlling harmful cyanobacterial blooms in a world experiencing anthropogenic and climatic-induced change, Science of The Total Environment, 409 (2011) 1739-1745.

[2] J. Patocka, The toxins of Cyanobacteria, Acta medica (Hradec Kralove) / Universitas Carolina, Facultas Medica Hradec Kralove, 44 (2001) 69-75.

[3] V. Gupta, S.K. Ratha, A. Sood, V. Chaudhary, R. Prasanna, New insights into the biodiversity and applications of cyanobacteria (blue-green algae) - Prospects and challenges, Algal Research, 2 (2013) 79-97.

[4] J.H. Landsberg, The Effects of Harmful Algal Blooms on Aquatic Organisms, Reviews in Fisheries Science, 10 (2002) 113-390.

[5] W.W. Carmichael, Health Effects of Toxin-Producing Cyanobacteria: "The CyanoHABs", Human and Ecological Risk Assessment: An International Journal, 7 (2001) 1393-1407.

[6] M.E. Van Apeldoorn, H.P. Van Egmond, G.J.A. Speijers, G.J.I. Bakker, Toxins of cyanobacteria, Molecular Nutrition and Food Research, 51 (2007) 7-60.

[7] J. Jia, W. Luo, Y. Lu, J.P. Giesy, Bioaccumulation of microcystins (MCs) in four fish species from Lake Taihu, China: Assessment of risks to humans, Science of The Total Environment, 487 (2014) 224-232.

[8] A. Zastepa, F.R. Pick, J.M. Blais, Fate and Persistence of Particulate and Dissolved Microcystin-LA from Microcystis Blooms, Human and Ecological Risk Assessment, 20 (2014) 1670-1686.

[9] R.M. Dawson, the toxicology of microcystins, Toxicon, 36 (1998) 953-962.

[10] S. Merel, D. Walker, R. Chicana, S. Snyder, E. Baurès, O. Thomas, State of knowledge and concerns on cyanobacterial blooms and cyanotoxins, Environment International, 59 (2013) 303-327.

[11] H. Choi, M.G. Antoniou, M. Pelaez, A.A. de La Cruz, J.A. Shoemaker, D.D. Dionysiou, Mesoporous nitrogen-doped TiO_2 for the photocatalytic destruction of the cyanobacterial toxin microcystin-LR under visible light irradiation, Environmental Science and Technology, 41 (2007) 7530-7535.

[12] C. Han, M. Pelaez, V. Likodimos, A.G. Kontos, P. Falaras, K. O'Shea, D.D. Dionysiou, Innovative visible light-activated sulfur doped TiO_2 films for water treatment, Applied Catalysis B: Environmental, 107 (2011) 77-87.

[13] C. Han, J. Andersen, V. Likodimos, P. Falaras, J. Linkugel, D.D. Dionysiou, The effect of solvent in the sol–gel synthesis of visible light-activated, sulfur-doped TiO_2 nanostructured porous films for water treatment, Catalysis Today, 224 (2014) 132-139.

[14] C.G. Silva, J.L. Faria, Photocatalytic oxidation of benzene derivatives in aqueous suspensions: Synergic effect induced by the introduction of carbon nanotubes in a TiO_2 matrix, Applied Catalysis B: Environmental, 101 (2010) 81-89.

[15] M.J. Sampaio, R.R.N. Marques, P.B. Tavares, J.L. Faria, A.M.T. Silva, C.G. Silva, Tailoring the properties of immobilized titanium dioxide/carbon nanotube composites for photocatalytic water treatment, Journal of Environmental Chemical Engineering, 1 (2013) 945-953.

[16] B. Gao, G.Z. Chen, G. Li Puma, Carbon nanotubes/titanium dioxide (CNTs/TiO_2) nanocomposites prepared by conventional and novel surfactant wrapping sol-gel methods exhibiting enhanced photocatalytic activity, Applied Catalysis B: Environmental, 89 (2009) 503-509.

[17] S. Morales-Torres, L. Pastrana-Martínez, J. Figueiredo, J. Faria, A.T. Silva, Design of graphene-based TiO_2 photocatalysts - a review, Environ Sci Pollut Res, 19 (2012) 3676-3687.

[18] L.M. Pastrana-Martínez, S. Morales-Torres, S.K. Papageorgiou, F.K. Katsaros, G.E. Romanos, J.L. Figueiredo, J.L. Faria, P. Falaras, A.M.T. Silva, Photocatalytic behaviour of nanocarbon–TiO_2 composites and immobilization into hollow fibres, Applied Catalysis B: Environmental, 142–143 (2013) 101-111.

[19] R.R.N. Marques, M.J. Sampaio, P.M. Carrapiço, C.G. Silva, S. Morales-Torres, G. Dražić, J.L. Faria, A.M.T. Silva, Photocatalytic degradation of caffeine: Developing solutions for emerging pollutants, Catalysis Today, 209 (2013) 108-115.

[20] M.J. Sampaio, C.G. Silva, R.R.N. Marques, A.M.T. Silva, J.L. Faria, Carbon nanotube–TiO_2 thin films for photocatalytic applications, Catalysis Today, 161 (2011) 91-96.

[21] H. Lim, S. Park, H. Cheong, Photoluminescence of Natural Diamonds, Journal of the Korean Physical Society, 48 (2006) 1556-1559.

[22] T. Fotiou, T.M. Triantis, T. Kaloudis, L.M. Pastrana-Martínez, V. Likodimos, P. Falaras, A.M.T. Silva, A. Hiskia, Photocatalytic degradation of microcystin-LR and off-odor compounds in water under UV-A and solar light with a nanostructured photocatalyst based on reduced graphene oxide-TiO_2 composite. Identification of intermediate products, Industrial and Engineering Chemistry Research, 52 (2013) 13991-14000.

[23] W.S. Hummers, R.E. Offeman, Preparation of Graphitic Oxide, Journal of the American Chemical Society, 80 (1958) 1339-1339.

[24] F. Rouquérol, J. Rouquérol, K.S.W. Sing, Adsorption by Powders and Porous Solids. principles, Methodology and Applications, Academic Press, London, 1999.

[25] S.J. Gregg, K.S.W. Sing, Adsorption, Surface Area and Porosity, Academic Press, New York, 1982.

[26] W.H. Organization, Guidelines for safe recreational water environments, Volume 1: Coastal and fresh waters. http://www.who.int/water_sanitation_health/bathing/srwe1/en/ (Accessed on December 2014)

[27] A.J. Maira, J.M. Coronado, V. Augugliaro, K.L. Yeung, J.C. Conesa, J. Soria, Fourier Transform Infrared Study of the Performance of Nanostructured TiO_2 Particles for the Photocatalytic Oxidation of Gaseous Toluene, Journal of Catalysis, 202 (2001) 413-420.

[28] G. Martra, Lewis acid and base sites at the surface of microcrystalline TiO_2 anatase: relationships between surface morphology and chemical behaviour, Applied Catalysis A: General, 200 (2000) 275-285.

[29] R. Yudianti, H. Onggo, Sudirman, Y. Saito, T. Iwata, J. Azuma, Analysis of Functional Group Sited on Multi-Wall Carbon Nanotube Surface, The Open Materials Science Journal, 5 (2011) 242-247.

[30] J.L. Figueiredo, M.F.R. Pereira, M.M.A. Freitas, J.J.M. Órfão, Modification of the surface chemistry of activated carbons, Carbon, 37 (1999) 1379-1389.

[31] J.L. Figueiredo, M.F.R. Pereira, M.M.A. Freitas, J.J.M. Órfão, Characterization of Active Sites on Carbon Catalysts, Industrial & Engineering Chemistry Research, 46 (2006) 4110-4115.

[32] L.M. Pastrana-Martínez, S. Morales-Torres, V. Likodimos, P. Falaras, J.L. Figueiredo, J.L. Faria, A.M.T. Silva, Role of oxygen functionalities on the synthesis of photocatalytically active graphene–TiO_2 composites, Applied Catalysis B: Environmental, 158–159 (2014) 329-340.

[33] P. Solís-Fernández, R. Rozada, J.I. Paredes, S. Villar-Rodil, M.J. Fernández-Merino, L. Guardia, A. Martínez-Alonso, J.M.D. Tascón, Chemical and microscopic analysis of graphene prepared by different reduction degrees of graphene oxide, Journal of Alloys and Compounds, 536, Supplement 1 (2012) S532-S537.

[34] R. Leary, A. Westwood, Carbonaceous nanomaterials for the enhancement of TiO_2 photocatalysis, Carbon, 49 (2011) 741-772.

[35] M.G. Antoniou, A.A. de La Cruz, D.D. Dionysiou, Intermediates and reaction pathways from the degradation of microcystin-LR with sulfate radicals, Environmental Science and Technology, 44 (2010) 7238-7244.

[36] M.G. Antoniou, J.A. Shoemaker, A.A. de La Cruz, D.D. Dionysiou, Unveiling New Degradation Intermediates/Pathways from the Photocatalytic Degradation of Microcystin-LR, Environmental Science & Technology, 42 (2008) 8877-8883.

[37] Y. Su, Y. Deng, Y. Du, Alternative pathways for photocatalytic degradation of microcystin-LR revealed by TiO_2 nanotubes, Journal of Molecular Catalysis A: Chemical, 373 (2013) 18-24.

[38] L. Ho, G. Onstad, U.v. Gunten, S. Rinck-Pfeiffer, K. Craig, G. Newcombe, Differences in the chlorine reactivity of four microcystin analogues, Water Research, 40 (2006) 1200-1209.

[39] M.G. Antoniou, J.A. Shoemaker, A.A. de La Cruz, D.D. Dionysiou, LC/MS/MS structure elucidation of reaction intermediates formed during the TiO_2 photocatalysis of microcystin-LR, Toxicon, 51 (2008) 1103-1118.

[40] M. Grootveld, B. Halliwell, Aromatic hydroxylation as a potential measure of hydroxyl-radical formation in vivo. Identification of hydroxylated derivatives of salicylate in human body fluids, Biochemical Journal, 237 (1986) 499-504.

[41] K. Kaya, T. Sano, A Photodetoxification Mechanism of the Cyanobacterial Hepatotoxin Microcystin-LR by Ultraviolet Irradiation, Chemical Research in Toxicology, 11 (1998) 159-163.

[42] S. Banerjee, S.C. Pillai, P. Falaras, K.E. O'Shea, J.A. Byrne, D.D. Dionysiou, New Insights into the Mechanism of Visible Light Photocatalysis, The Journal of Physical Chemistry Letters, 5 (2014) 2543-2554.